

Ionospheric Effects on SAR Imaging: A Numerical Study

Jun Liu, Yasuo Kuga, *Senior Member, IEEE*, Akira Ishimaru, *Life Fellow, IEEE*, Xiaoqing Pi, and Anthony Freeman, *Fellow, IEEE*

Abstract—There has been an increasing interest in the use of spaceborne very high frequency ultra high frequency (VHF-UHF) synthetic aperture radar (SAR) for measuring forest biomass and for detecting underground facilities. The propagation characteristics of the low-frequency electromagnetic wave are severely affected by the ionosphere. Recently, Faraday rotation effects and SAR image degradation have been studied using an analytical model and a homogeneous ionosphere. In this paper, a numerical model is developed to investigate the SAR image degradation caused by an inhomogeneous ionosphere. Both horizontal and vertical structures of the ionosphere are considered in this model. Three different cases are studied. The first is a vertically homogeneous ionosphere, where the simulation condition is the same as in the analytical study by Ishimaru and others. The second is a vertical profile, which is introduced using the Chapman formula. The ray-bending effect is added for the ionosphere with a layered structure. Finally, both the vertical profile in electron density and the horizontal gradient in total electron content are considered in the simulation. Simulation results show good agreement with the theoretical analysis under the same conditions of the ionosphere. When both horizontal and vertical structures and the inhomogeneity of the ionosphere are considered in the model, the simulation result shows further image degradation and shift caused by the ray-bending effect. The simulation results also show the strong frequency dependence of the SAR image resolution.

Index Terms—Ionospheric electromagnetic propagation, remote sensing, synthetic aperture radar (SAR).

I. INTRODUCTION

THERE HAS BEEN an increasing interest in the use of spaceborne very high frequency ultra high frequency synthetic aperture radar (VHF-UHF SAR) for measuring forest biomass and for detecting underground facilities which requires the use of longer wavelengths for enhanced foliage and ground penetration [1]. SAR provides high-resolution images by coherently processing the signals returned from the ground. Perturbations in the signal propagation path, including the ionosphere and troposphere, lead to phase change within the effective aperture of the system. This phase perturbation caused by the irregularities of the refractive index structure of the ionosphere will be particularly severe at VHF-UHF frequency and will distort the SAR image. These effects as well

as possible mitigation techniques must be investigated before deploying a VHF-UHF SAR in space.

In our previous analytical study [2], a homogeneous layer of constant electron density for the ionosphere is assumed. The average electron density is specified, and the irregularity of the ionosphere is given by a two-parameter spectrum. The SAR image resolutions were then obtained by computing the 3-dB width of the second order of the ambiguity function. Results indicate a substantial change in azimuthal resolution for the UHF-band SAR system, while the change of range resolution is negligible. However, the real ionosphere is not uniform and has both small- and large-scale structures, mostly due to ionospheric dynamical processes, plasma instabilities, and the coupling between ionosphere, thermosphere, and magnetosphere [3]–[5]. Two factors may affect the SAR imaging: 1) ambient total electron current (TEC) on large spatial scales greater than a few hundred kilometers, and 2) irregularities on scales from a few meters to a few tens of kilometers. The former can have large gradient and curvature, such as in the equatorial anomaly region, while the latter can occur mostly in the equatorial and auroral regions (less frequently at middle latitudes).

Our previous study also assumes that the ionosphere is vertically uniform, but in reality, the electron density varies with height and its peak value appears at around 300-km altitude. The vertical structure of the ionosphere introduces a ray-bending effect which causes both image degradation and image shift. In addition to the random variation of the electron density, a horizontal total electron content gradient may also exist within the SAR aperture.

In this paper, a numerical model is developed to evaluate these potential effects. The horizontal structure is described using a two-parameter spectrum. As for the vertical profile, three different cases are studied. First, a vertically homogeneous ionosphere is considered. The simulation condition is the same as in the analytical study. The purpose of this case is to compare simulation results with analytical results and determine good agreement. Second, a vertical profile is introduced using the Chapman formula. The ray-bending effect is added for an ionosphere with a layered structure. Third, both vertical profile and TEC slope are considered in the simulation.

II. DESCRIPTION OF THE MODEL

For SAR applications, spatial variations of electron density and TEC along and among radio ray paths from the ground to the SAR satellite must be considered. A two-dimensional ionosphere structure in the orbital plane is assumed. The image is

Manuscript received August 14, 2002; revised January 28, 2003. This work was supported by Jet Propulsion Laboratory under the JPL/NASA ARTP Program.

J. Liu, Y. Kuga, and A. Ishimaru are with the Department of Electrical Engineering, University of Washington, Seattle, WA 98195-2500 USA.

X. Pi and A. Freeman are with the Jet Propulsion Laboratory, California Institute of Technology, Pasadena, CA 91109 USA.

Digital Object Identifier 10.1109/TGRS.2003.811813

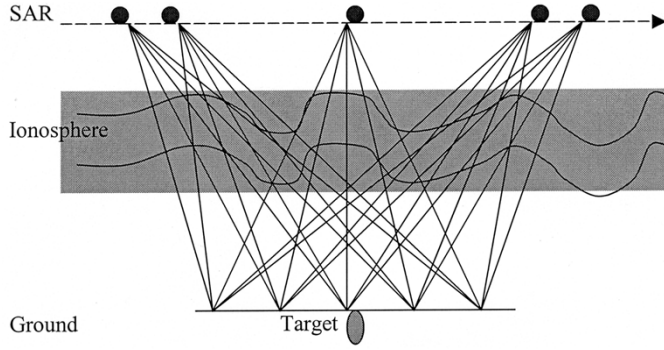


Fig. 1. SAR flight path and ground target.

constructed within the plane formed by the satellite track and the wave propagation path. We assume the equivalent aperture size of the SAR system is 10 km, the data sampling distance along the flight path is 100 m, the number of sampling points is 100, the altitude of the satellite orbit is 400 km, and the SAR look angle is 60° . These parameters are based on the preliminary study of proposed UHF-band SAR by the Jet Propulsion Laboratory (JPL). The length of the ground to be observed is 1000 m. The data sampling distance on the ground is 10 m, which gives the number of sampling points to be 100. Fig. 1 shows the structure of the model. The Chapman formula will be used to describe the vertical profile of the ionosphere. A horizontal electron density perturbation is given by the two-parameter spectrum [2], [8]. The details will be discussed in the following section.

III. FORMULATION

The numerical model presented in this paper is based on the analytical model published in our previous paper [2]. Therefore, we will only briefly describe the analytical model.

A. Formula Used for Analytical Study

As a starting point, we assume the ionosphere is vertically uniform, and the random fluctuation is specified by the two-parameter spectrum of the refractive index fluctuation [7], [8]. In the analytical study, the SAR image characteristics are given by the first- and second-moments of the generalized ambiguity function (system point target response) which is given by

$$\chi(\mathbf{r}, \mathbf{r}_0) = \sum_n \frac{1}{2\pi} \int \bar{g}_n(\omega, r_n) \bar{f}_n^*(\omega, r_{0n}) d\omega \quad (1)$$

where

$$\bar{g}_n(\omega, r_n) = \bar{u}_i(\omega) \bar{G}_0(\omega, r_n) \quad (2)$$

$$\bar{f}_n(\omega, r_{0n}) = \bar{u}_i(\omega) \exp\left(i\frac{\omega}{c} 2r_{0n}\right) \quad (3)$$

$$\bar{G}_0(\omega, r_n) = \frac{\exp(i2 \int \beta ds + \psi_{\text{down}} + \psi_{\text{up}})}{(4\pi r_n)^2} \quad (4)$$

Equation (1) is expressed in the frequency-domain, and u_i , G_0 , and f_n are the Fourier transform of the input signal, Green's function, and matched filter function, respectively. The propagation constant along the electromagnetic wave path is $\beta(\omega)$, and ψ_{down} and ψ_{up} are the down- and up-path complex phase fluctuations due to the ionospheric turbulence.

By combining (1)–(4) and using $\psi = \psi_{\text{down}} = \psi_{\text{up}}$, we can obtain

$$\chi(\mathbf{r}, \mathbf{r}_0) = \sum_n \frac{1}{2\pi} \int \bar{u}_i(\omega)^2 \frac{\exp\left(i2 \int \beta ds - i\frac{\omega}{c} 2r_{0n} + 2\psi\right)}{(4\pi r_n)^2} d\omega. \quad (5)$$

$\beta(\omega)$ can be expanded about the carrier frequency ω_0

$$\beta(\omega) = \beta(\omega_0) + (\omega - \omega_0)\beta'(\omega_0) + \frac{(\omega - \omega_0)^2}{2}\beta''(\omega_0) \quad (6)$$

where the first, second, and third terms are related to free-space propagation, group delay, and pulse broadening given in (9), (10), and (11), respectively. The input pulse $u_i(t)$ is usually a chirp signal. Using the Gaussian approximation, the Fourier transform of $u_i(t)$ can be expressed as [9]

$$\bar{u}_i(\omega) = \sqrt{\frac{\pi}{\alpha}} \exp\left[-\frac{(\omega - \omega_0)^2}{4\alpha}\right] \quad (7)$$

$$\alpha = \alpha_R + i\alpha_I = \frac{\pi}{4T_0^2} + i\frac{B}{4T_0}$$

where B is the bandwidth and T_0 is the pulse duration.

Then the signal observed at the n th position is given by

$$\chi_n(r_n, r_{0n}) = \frac{1}{(4\pi r_n)^2} \exp(i\Phi_0(\omega_0)) \cdot \int \exp\left(i(\omega - \omega_0)\Phi_1 - (\omega - \omega_0)^2\Phi_2\right) d\omega \quad (8)$$

$$\Phi_0(\omega_0) = 2\frac{\omega_0}{c}(r_n - r_{0n} - d_i) + 2\beta(\omega_0)d_i + 2\psi \quad (9)$$

$$\Phi_1(\omega_0) = \frac{2}{c}(r_n - r_{0n}) + 2\left[\beta'(\omega_0) - \frac{1}{c}\right]d_i \quad (10)$$

$$\Phi_2(\omega_0) = \frac{\alpha_R}{2|\alpha|^2} - i\beta''(\omega_0)d_i \quad (11)$$

where $d_i = \int ds$ the ionospheric thickness along the path, and Φ_0 determines the azimuthal resolution. The group delay is represented by Φ_1 , and Φ_2 represents the pulse broadening. Finally, the generalized ambiguity function is given by

$$\chi(\mathbf{r}, \mathbf{r}_0) = \sum_n \frac{1}{(4\pi r_n)^2} \exp(i\Phi_0(\omega_0)) \cdot \int \exp\left(i(\omega - \omega_0)\Phi_1 - (\omega - \omega_0)^2\Phi_2\right) d\omega. \quad (12)$$

The SAR image resolution and shift can be obtained from the first and second moments of (12) [2]. ψ represents the random fluctuation of the ionosphere and can be expressed in terms of the spectrum of the refractive index fluctuation and the structure function [10].

B. Model for Numerical Simulation

In the numerical model, the random fluctuation of ionospheric density affects the propagation constant β that contains the random perturbation in refractive index n . For a given electron density profile, we need to calculate the phase shift using β along the EM wave path. Therefore, the numerical simulation involves three steps. First, the electron density profile must be specified. Second, the refractive index along

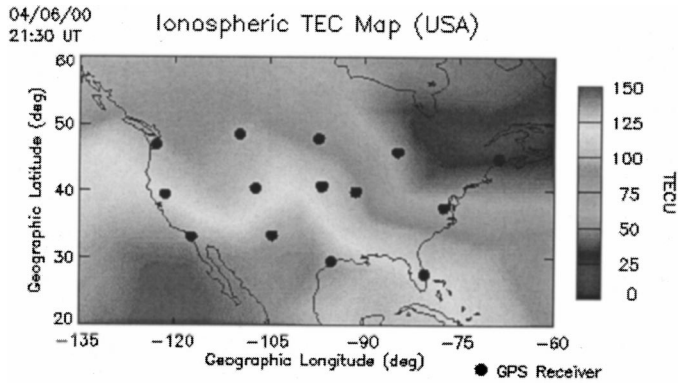


Fig. 2. An example of vertical TEC map over the United States and adjacent regions. The map was produced in real time on April 6, 2000, at JPL using GPS data measured from a regional ground receiver network. Ten degrees in latitude corresponds to 1180 km in an ionospheric altitude (~ 400 km) approximately.

the signal path must be calculated. Third, the SAR image must be formed for a given ionosphere profile.

Fig. 2 is an example of a TEC map produced by the JPL using dual-frequency global positioning system (GPS) data collected from a regional ground-GPS receiver network. The map represents vertical TEC (altitude integration of electron densities) up to the orbit height of GPS satellites. The map shows horizontal gradient structures that can occur under disturbed space weather conditions. In addition to the large-scale structures shown in the TEC map, small- and medium-scale (meter to kilometer) electron density and TEC irregularities can also occur [3]. Since the SAR aperture size is on the order of *kilometers*, it is also necessary to investigate the possible impact on the SAR imaging caused by this TEC gradient within the radar aperture.

To generate random fluctuations of electron density, we will use the technique developed for a random surface generation for the numerical simulations of wave scattering from rough surfaces [6]. This method uses the spectral density of the random surface to generate a surface profile which obeys a desired statistical function. Because a two-parameter spectrum was used in our analytical paper, we will generate an electron density profile with the same spectrum. The two-parameter spectrum in three-dimensional (3-D) κ space is given by [2], [8]

$$\Phi_N(\kappa) = \frac{A}{[\kappa^2 + \kappa_0^2]^{2\nu_1}}, \quad \text{for } \kappa \leq \kappa_b \quad (13)$$

$$\Phi_N(\kappa) = A [\kappa_0^2 + \kappa_b^2]^{2\nu_2 - \nu_1} [\kappa_0^2 + \kappa^2]^{-\nu_2}, \quad \text{for } \kappa > \kappa_b \quad \kappa_b = \frac{2\pi}{L_b} \kappa_0 = \frac{2\pi}{L_0} \quad (14)$$

where κ_b is a break wave number; L_0 is outerscale 10 km; L_b is breakscale 500 m; $2\nu_1 = 3.5$; and $2\nu_2 = 5.5$.

Our numerical simulation requires a two-parameter spectrum expressed in one-dimensional (1-D) κ space. The relationship between a 1-D and 3-D spectrum is given by [10]

$$\Phi_N(\kappa) = -\frac{1}{2\pi\kappa} \frac{\partial V(\kappa)}{\partial \kappa} \quad (15)$$

where $V(\kappa)$ is the two-parameter spectrum expressed in 1-D κ space

$$V(\kappa) = \frac{\pi A}{\nu_1 - 1} \frac{1}{[\kappa^2 + \kappa_0^2]^{(\nu_1 - 1)}} - \frac{\pi A}{(\kappa_b^2 + \kappa_0^2)^{\nu_1 - 1}} \cdot \left(\frac{1}{\nu_1 - 1} - \frac{1}{\nu_2 - 1} \right), \quad \text{for } \kappa \leq \kappa_b \quad (16)$$

$$V(\kappa) = \frac{\pi A [\kappa_0^2 + \kappa_b^2]^{2\nu_2 - \nu_1}}{\nu_2 - 1} \cdot \frac{1}{[\kappa^2 + \kappa_0^2]^{(\nu_2 - 1)}}, \quad \text{for } \kappa > \kappa_b. \quad (17)$$

To generate an electron density profile numerically, a sequence of normally distributed random numbers is used in the phase of the profile spectrum. The profile $N_z = f(x_n)$ is related to the 1-D discrete Fourier transform of the profile spectrum as described in the following equations:

$$f(x) = \frac{1}{L} \sum_{n=-N/2}^{(N/2)-1} F(K_n) \exp(iK_n x) \quad (18)$$

where

$$F(K_n) = \sqrt{2\pi L V(K_n)} \cdot \begin{cases} \frac{1}{\sqrt{2}} [N(0, 1) + iN(0, 1)], & n \neq 0, N/2 \\ N(0, 1), & n = 0, N/2 \end{cases} \quad (19)$$

$$K_n = \frac{2\pi n}{L} \quad i = \sqrt{-1}.$$

$N(0, 1)$ denotes a sequence of normally distributed numbers in $[0, 1]$ with zero mean and unity standard deviation. L is a total length of a profile. It can be seen that the two-point statistics are governed by the magnitude of the Fourier spectrum which follows the profile spectrum $V(\kappa)$, and the one-point statistics are governed by the random modulation in the phase of the Fourier coefficients. The profile is a series of real numbers; therefore, the phase of the Fourier coefficient must satisfy the following requirements

$$F(K_n) = F^*(-K_n). \quad (20)$$

Fig. 3 shows a typical profile generated with this method. In this model, the average peak electron density of the ionosphere is set to 10^{12} el/m³. The average vertical TEC, electron density integration up to a typical SAR orbit altitude (set to be 400 km above ground in this study) is set to 5 TECU where TECU = 10^{16} el/m². One realization has 100 points along the satellite track with 100 m per point. In our previous analytical studies, we assumed that the ionosphere is vertically uniform to simplify the analysis. The actual ionosphere, however, has a vertical profile which must be included in the numerical simulations. We use the Chapman formula to describe the vertical electron density profile of the ionosphere [8]. A typical daytime electron density N_e profile is given as

$$z = \frac{h - H_{\max}}{H_{\text{scale}}} \quad (21)$$

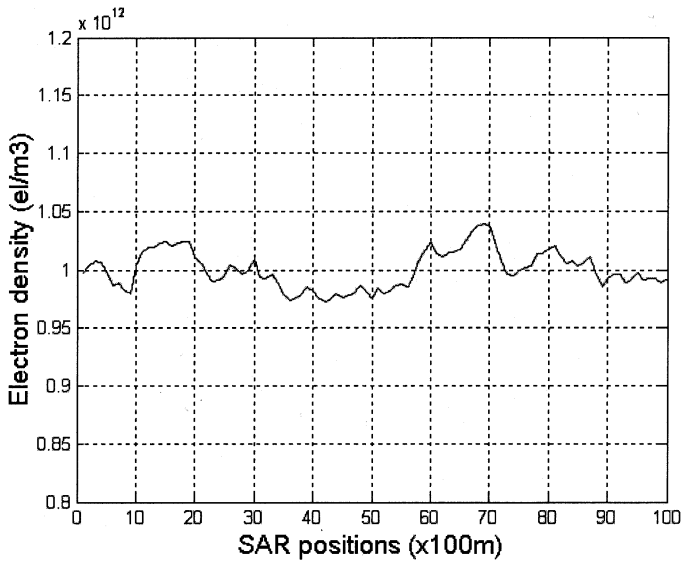


Fig. 3. Horizontal electron density profile generated using the two-parameter spectrum. Average peak value = 10^{12} el/m³. Average TEC = 5 TECU and perturbation = 10%. Ionosphere thickness = 50 km. TEC = (average electron density) * (ionosphere thickness)/TECU. TECU = 10^{16} el/m².

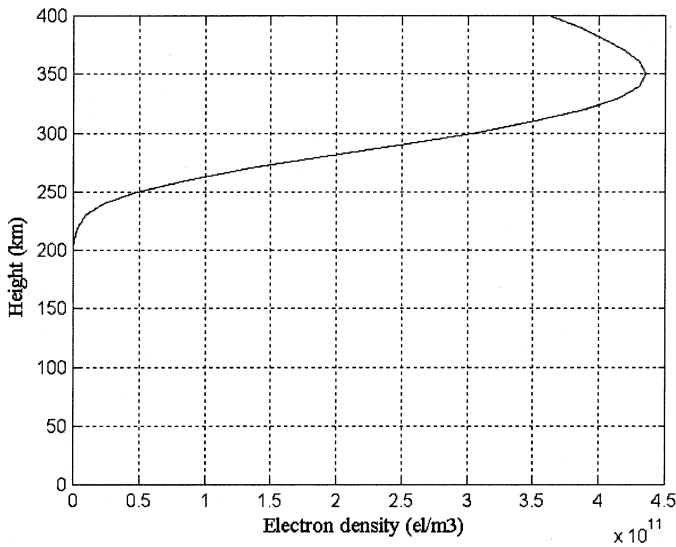


Fig. 4. Vertical electron density profile up to the assumed SAR altitude, generated using the Chapman formula.

and

$$N_e = N_{\max} \exp(0.5(1.0 - z - e^{-z})). \quad (22)$$

H_{\max} is the height where N_e has maximum value. H_{scale} determines the sharpness of the shape. $H_{\max} = 350$ km and $H_{\text{scale}} = 50$ km are used in our simulations. Fig. 4 shows the vertical electron density generated by the Chapman formula using these parameters.

The next step is to calculate the refractive index profile from a given electron density profile. Because of the presence of the earth's geomagnetic field, both ordinary and extraordinary modes with a different index of refraction will be present within the ionosphere. To simplify the problem, we assume the wave is propagating in the z direction and the geomagnetic field H_{dc} is in the $y-z$ plane as shown in Fig. 5 [8].

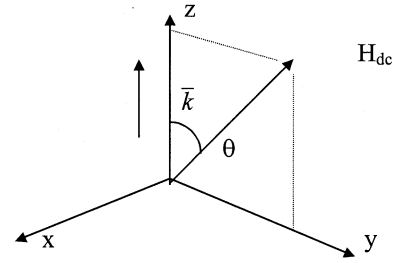


Fig. 5. Coordinate system used in the model. Wave is propagating in z direction. H_{dc} is the geomagnetic field.

Then the index of refraction for both ordinary and extraordinary modes for each layer can be expressed as [2]

$$n^2 - 1 = - \frac{X}{U + \frac{Y_y^2}{2(X-U)} \mp \sqrt{\frac{Y_y^4}{4(X-U)^2} + Y_z^2}} \quad (23)$$

where $X = \omega_p^2/\omega^2$; $Y = \epsilon\mu_0 H_{\text{dc}}/m_e\omega$; $Y_z = Y \cos\theta$; $Y_y = Y \sin\theta$; $U = 1 - j\nu/\omega$; ν is the collision frequency; m_e is the mass of the electron; μ_0 is the permeability of the free space; and the plasma frequency is given as $\omega_p = 2\pi f_p = 2\pi \times 8.98 \times (N_e)^{0.5}$.

The last step is to describe the generalized ambiguity function in the numerical model. The random fluctuation of the ionosphere affects the propagation constant β that contains the refractive index fluctuation n . For a given electron density profile, we need to calculate the phase shift using β along the signal path.

We now express (4) as

$$\overline{G}_0(\omega, r_n) = \frac{\exp(i2 \int \beta ds)}{(4\pi r_n)^2}. \quad (24)$$

Therefore, (5) will be modified as

$$\chi(\mathbf{r}, \mathbf{r}_0) = \sum_n \frac{1}{2\pi} \int \overline{u}_i(\omega)^2 \frac{\exp(i2 \int \beta ds - i\frac{\omega}{c} 2r_{0n})}{(4\pi r_n)^2} d\omega \quad (25)$$

and (9) becomes

$$\Phi_0(\omega_0) = 2\frac{\omega_0}{c} \left(r_n - r_{0n} - \sum_{i=1,m} \Delta d_i \right) + 2 \sum_{i=1,m} \beta_i(\omega_0) \Delta d_i. \quad (26)$$

Finally, the generalized ambiguity function is given by

$$\chi(\mathbf{r}, \mathbf{r}_0) = \sum_n \frac{1}{(4\pi r_n)^2} \exp(i\Phi_0(\omega_0)) \quad (27)$$

where m is the number of layers in which the ionosphere is divided; β_i is the propagation constant of the i th layer; and Δd_i is the thickness of each layer.

It should be noted that the process described in this section will generate a SAR image for one realization of the ionosphere. To obtain the statistical data and SAR image, more than 100 realizations must be computed for the given average TEC and perturbation values.

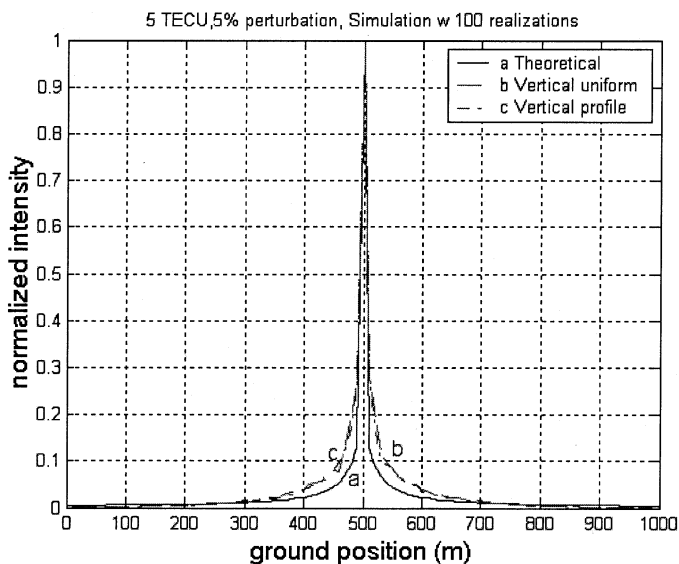


Fig. 6. Case 1. Comparison between theoretical and numerical results. SAR frequency is 500 MHz. Average TEC = 5 TECU and 5% perturbation.

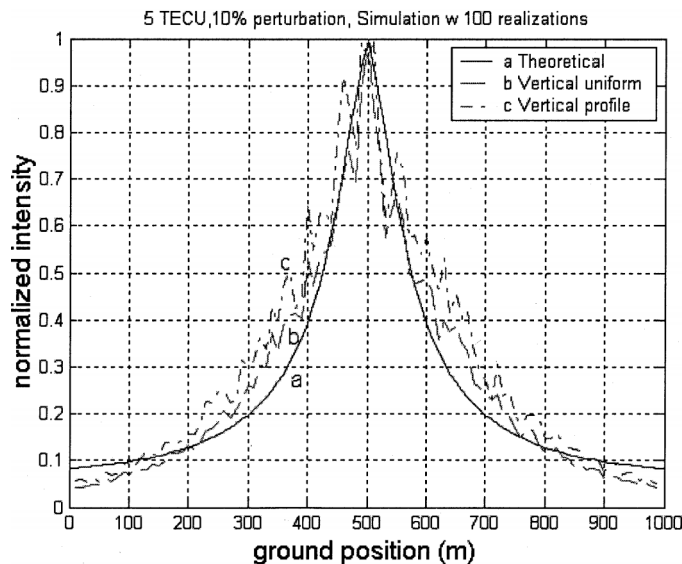


Fig. 7. Case 2. Comparison between theoretical and numerical results. SAR frequency is 500 MHz. Average TEC = 5 TECU and 10% perturbation.

IV. CASE STUDIES

Numerical simulations are conducted for three different cases. The vertically uniform profile is used for comparison with the analytical study. The ionosphere with a vertical profile and slant TEC slope profiles is for more realistic cases.

A. Vertically Uniform Electron Density Distribution

The main purpose of this case is to verify the numerical model by comparing it with the previous analytical calculations. In our analytical studies, a homogenous layer of constant electron density for the ionosphere is assumed. The average electron density is specified, and the irregularities of the ionosphere are given by the two-parameter spectrum. The SAR image resolutions were then obtained by computing the 3-dB width of the second-order moment of the ambiguity function. It is expected that under the same ionospheric conditions, the simulation results should have good agreement with the analytical results.

The ionosphere is specified by a uniform 50-km-thick slab. The average electron density at each point within this slab is constant. The entire ionosphere acts as one layer and, therefore, there is no ray-bending within the ionosphere. In the numerical model, however, the uniform ionosphere is divided into many vertical layers. Each layer contributes to the image distortion and the effects must be added together. The image is formed by coherently summing signals from each SAR sample point.

Figs. 6–9 show SAR images of four different numerical results is due to the slow convergence of the averaging processionosphere conditions. The solid line in each plot corresponds to the analytical result. The dashed line represents the numerical result for an ionosphere with a uniform vertical structure. Also shown are the numerical results with the vertical electron density profile which will be discussed in the following section. In all cases, the numerical results of the uniform ionosphere are close to those of the analytical results indicating the validity of our simulations. The fluctuation in the. The 3-dB image resolution of Fig. 6 (TEC = 5 TECU, TEC perturbation = 5%) is al-

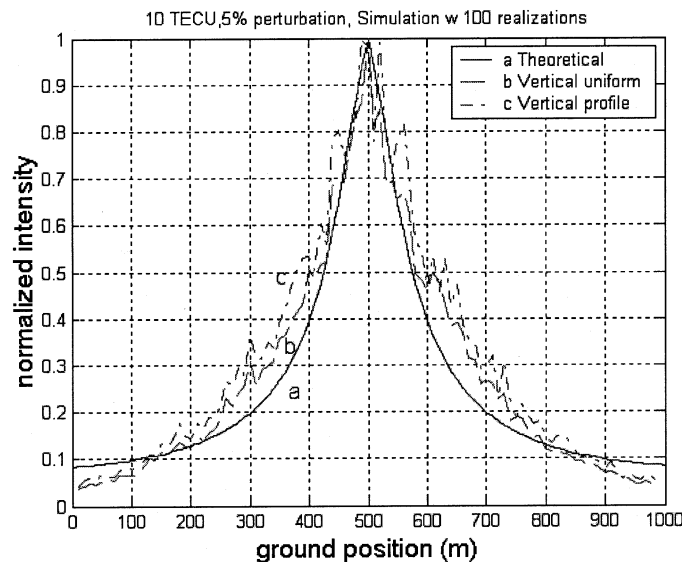


Fig. 8. Case 3. Comparison between theoretical and numerical. SAR frequency is 500 MHz. Average TEC = 10 TECU and 5% perturbation.

most the same as the free-space image resolution indicating the small effects of the ionosphere. Increasing both average TEC and perturbation values, however, will result in a substantial degradation of the image resolution as shown in Figs. 7–9. The values used in Fig. 9 (TEC = 10 TECU, TEC perturbation = 10%) are not unusual during the day time. It is obvious that the 3-dB spread of 480 m shown in Fig. 9 will be unacceptable for most practical SAR imaging situations.

B. Ionosphere With Vertical Profile

The purpose of studying an ionosphere with a vertical profile is to simulate more realistic cases and also to analyze the ray-bending effects [11]. The vertical profile is specified by the Chapman formula and shown in Fig. 4. The ionosphere is vertically sliced into many layers, and the index of refraction of each layer is calculated from the electron density. Because the index

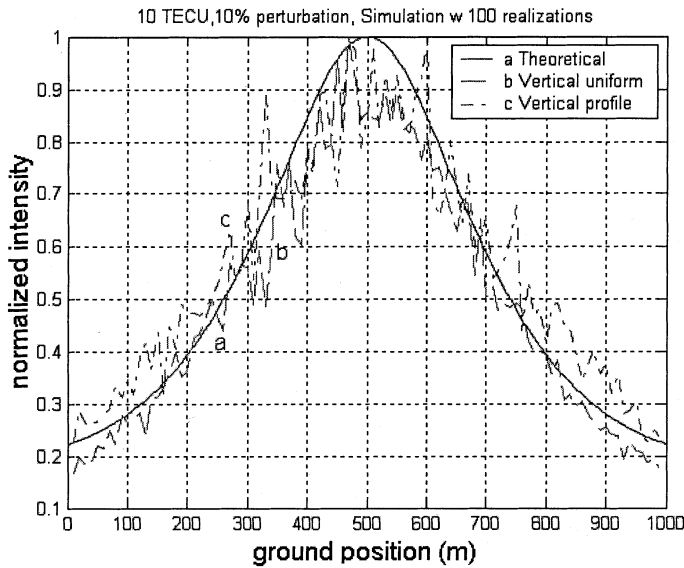


Fig. 9. Case 4. Comparison between theoretical and numerical. SAR frequency is 500 MHz. Average TEC = 10 TECU and 10% perturbation.

TABLE I
SAR IMAGE RESOLUTION FOR DIFFERENT CASES: ANALYTICAL, VERTICAL UNIFORM, AND VERTICAL PROFILE

	Case 1			Case 2			Case 3			Case 4		
N	5 TECU			5 TECU			10 TECU			10 TECU		
D _N	5%			10%			5%			10%		
	a	b	c	a	b	c	A	b	c	a	b	c
W _{3dB} (m)	5	5	5	150	160	200	140	160	200	480	480	520

Note: N: TEC, D_N: TEC perturbation, W_{3dB}(m): 3 dB spread.

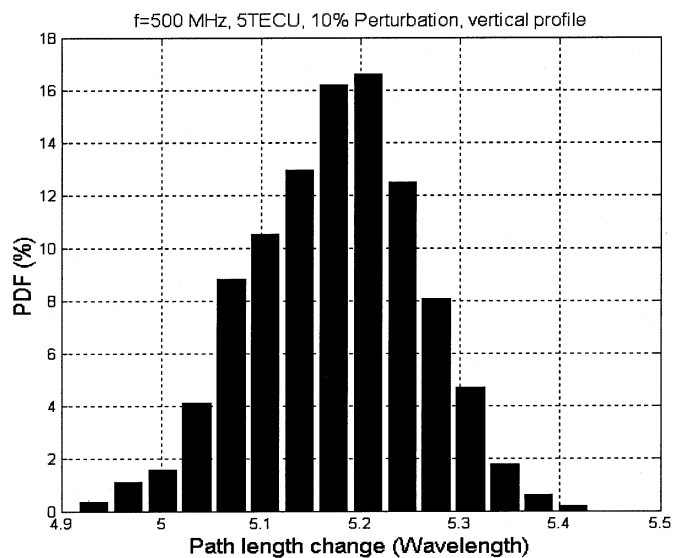


Fig. 10. PDF of path length change due to ray-bending with TEC perturbation (one-way only). SAR frequency is 500 MHz. Average TEC = 5 TECU and 10% perturbation.

of refraction changes along the signal path, ray-bending due to refraction at boundaries occurs. This ray-bending will be an additional cause of SAR image degradation and image shift. The dashed-dotted line in Figs. 6–9 represents simulation results for

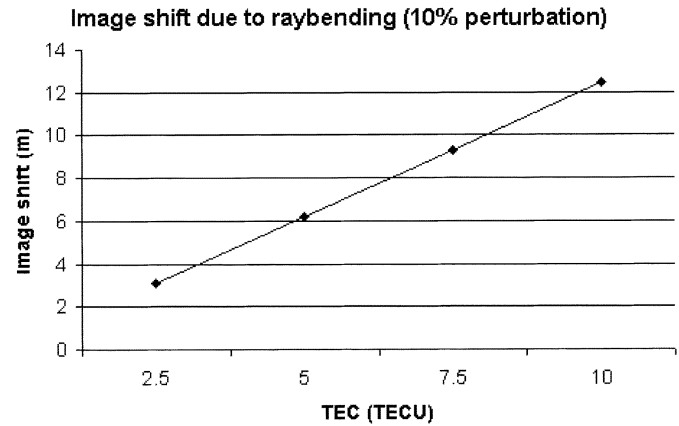


Fig. 11. Image shift due to ray-bending for different TEC. SAR frequency is 500 MHz. Ten percent perturbation is assumed.

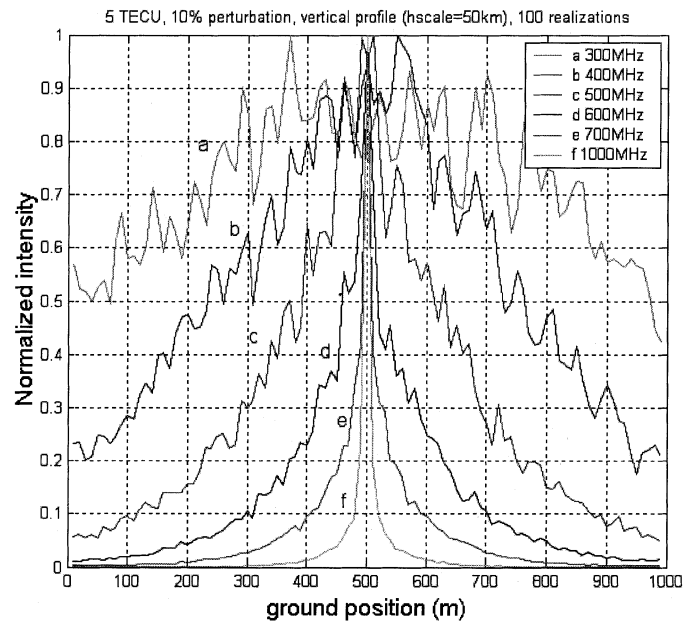


Fig. 12. SAR image resolution in the ionosphere for different operating frequency. Average TEC = 5 TECU and 10% perturbation.

an ionosphere with a vertical electron density profile. In general, the effect of the vertical profile compared to the uniform case is small. Table I summarizes the simulation results of four TEC cases.

Without the TEC perturbation, the ray-bending does not create SAR image degradation because each individual path goes through an ionosphere that has the same vertical refraction index distribution. However, when the TEC perturbation is added to the model, the refraction index distribution of each signal path will be different. Consequently, the phase shift caused by the ray-bending effect for each path will also be different. Fig. 10 shows the probability density function (pdf) of the path length change with respect to that of the straight ray along the SAR aperture. The ray-bending creates an average change of 5.17λ . In addition, the ionosphere perturbation will create a standard deviation of approximately 0.082λ . The variation in path length among the received signals will introduce phase incoherency, and therefore, degrade the SAR image resolution. Without the TEC perturbation, the same pdf

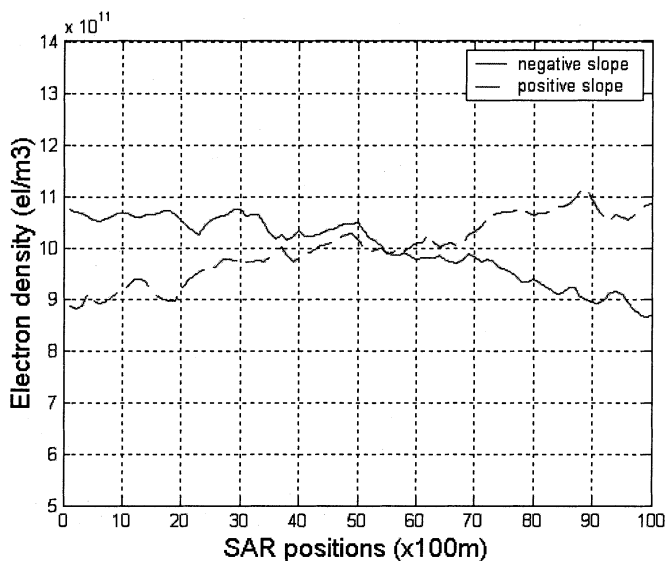


Fig. 13. Horizontal electron density profile with ± 2 TECU/10-km slope. The Chapman formula is used for a vertical profile. Average TEC = 5 TECU and perturbation = 10%.

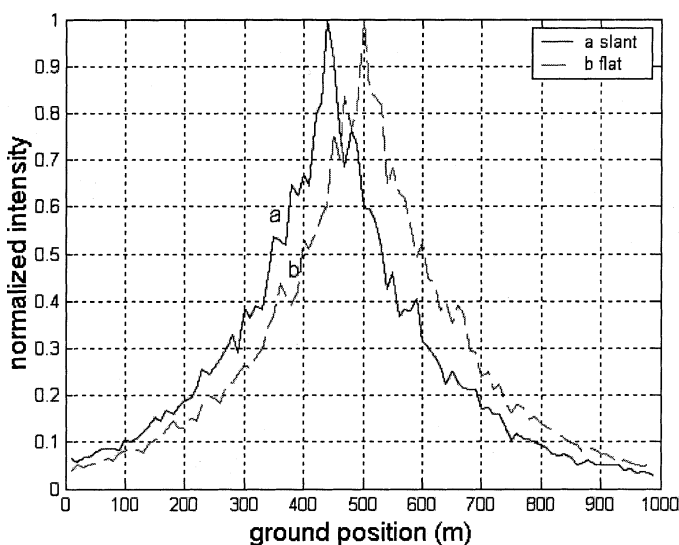


Fig. 14. Image shift. Horizontal TEC profile with 2-TECU/10-km slope. SAR frequency is 500 MHz. Average TEC = 5 TECU and perturbation = 10%.

shows a single peak at 5.17λ as expected. The ray-bending effect also causes an image shift in range direction. Fig. 11 shows that the expected image shift will be less than 10 m for TEC perturbations assumed here. The image broadening in the range direction is negligible, as it has been pointed out that the standard deviation is on the order of $10^{-2} \lambda$ range [2].

Based on the previous study, it is known that the SAR image degradation is usually negligible above 1 GHz, but the effects become critical below 500 MHz. Fig. 12 shows SAR images for frequencies from 0.3–1 GHz for relatively small TEC values (average TEC = 5 TECU, TEC perturbation = 10%). The impact of the ionospheric variations on the SAR image resolution decreases to a negligible level for frequencies above 600 MHz. We also note that there exists a sharp transition from 400–600 MHz which is in good agreement with the analytical studies [2].

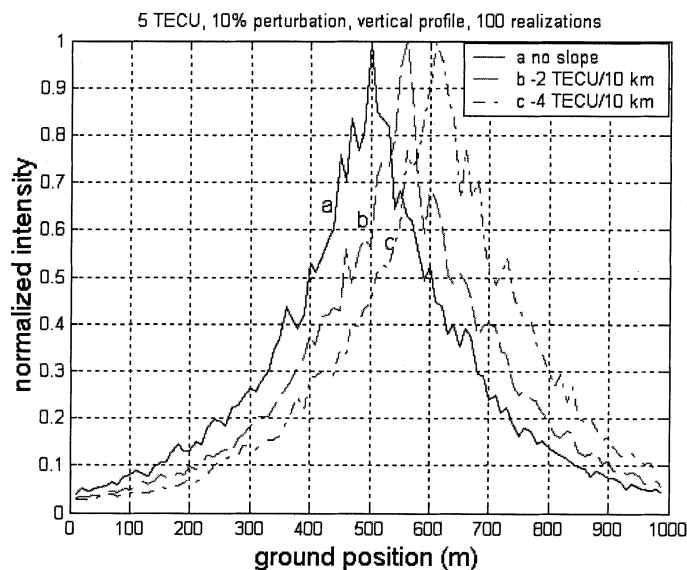


Fig. 15. Image shift. Horizontal TEC profile with different slopes. SAR frequency is 500 MHz. Average TEC = 5 TECU and perturbation = 10%.

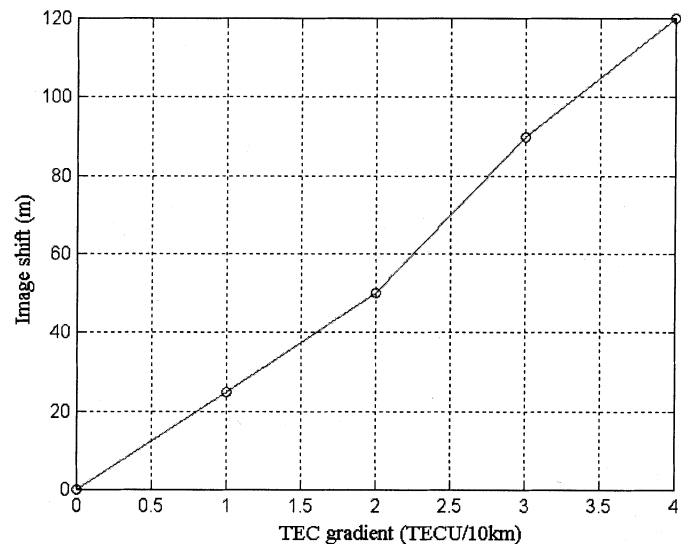


Fig. 16. Image shift versus TEC gradient. SAR frequency is 500 MHz. Average TEC = 5 TECU and perturbation = 10%.

C. Ionosphere With Slant TEC Slope

A typical TEC map shown in Fig. 2 indicates that a large scale TEC gradient can exist within the SAR aperture. To investigate the possible impact of the TEC slope as well as the TEC perturbation and vertical profile on the SAR imaging, a horizontal TEC gradient is added to the model. Both positive and negative gradients are studied, and these cases are shown in Fig. 13. Fig. 14 shows the result for the case with a positive TEC gradient with the average TEC = 5 TECU and TEC perturbation = 10%. The TEC gradient introduces an image shift, and the direction of the image shift depends on the sign of slope. Fig. 15 shows the image for three different slopes: 1) TEC slope = -0 TECU/10 km, 2) TEC slope = -2 TECU/10 km, and 3) TEC slope = -4 TECU/10 km. The expected image shift for different TEC gradients is shown in Fig. 16. An image shift of 100 m is possible for a relatively

quiet ionosphere (average TEC = 5 TECU and 10% TEC perturbation).

V. CONCLUSION AND DISCUSSION

The results presented in this paper clearly show that the inhomogeneous nature of the ionosphere must be included when estimating the SAR image degradation below 500 MHz. Because it is difficult to include the spatial and temporal variations of the ionosphere in an analytical model, development of an accurate numerical model will be essential. The model presented in this paper includes both horizontal and vertical profiles. The numerical model was verified with the analytical results for a homogeneous ionosphere. In addition, the simulations results indicate the following.

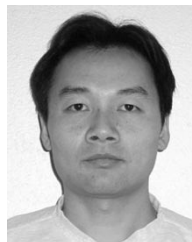
- When a vertical structure of the ionosphere is considered, further image degradation and image shift will be caused by the ray-bending effect.
- Ray-bending causes an average path length change of 5.17λ ($f = 500$ MHz) and image shift of 6 m for an ionosphere with average TEC (5 TECU) and 10% variation.
- In the presence of the TEC gradient within the SAR aperture, the image shifts in the azimuth direction can be 20 m for 1 TECU/10 km and up to 120 m for 4 TECU/10 km.
- The SAR image degradation caused by a structured ionosphere shows strong frequency dependence. The impact of the ionospheric variations on the SAR image resolution decreases to a negligible level for frequencies above 600 MHz. The frequency range from 600–400 MHz is a transition zone where image resolution degrades dramatically as frequency decreases. Our example shows the 3-dB image width increases from approximately 20 m at 600 MHz to 420 m at 400 MHz (Fig. 9).
- Ionospheric effects are negligible for an ionosphere with low average TEC (less than 5 TECU) and low perturbation (less than 5%).

One method to avoid the SAR image degradation is to collect data during the period when the ionosphere is relatively stable. The simulation results indicate that for a small TEC value and perturbation, such as the case with 5 TECU (integrated from the ground to 400-km SAR altitude) and 5% perturbation, the image degradation and the image shift are not significant. To mitigate the SAR image degradation, it may be necessary to obtain detailed information of the structure of the ionosphere. Although we have not studied a method to compensate for the ionospheric effects on SAR, the numerical model presented in this paper will be useful for testing different mitigation techniques.

REFERENCES

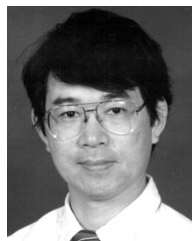
- [1] E. Rignot, J. R. Zimmermann, and J. J. Vanzyt, "Spaceborne applications of P-band imaging radars for measuring forest biomass," *IEEE Trans. Geosci. Remote Sensing*, vol. 33, pp. 1162–1169, Sept. 1995.
- [2] A. Ishimaru, Y. Kuga, J. Liu, Y. Kim, and T. Freeman, "Ionospheric effects on synthetic aperture radar imaging at 100 MHz to 2 GHz," *Radio Sci.*, vol. 34, no. 1, 1999.
- [3] X. Pi, A. J. Mannucci, U. J. Lindqwister, and C. M. Ho, "Monitoring of global ionospheric irregularities using the worldwide GPS network," *Geophys. Res. Lett.*, vol. 24, pp. 2283–2286, 1997.

- [4] M. Mendillo, J. Baumgardner, X. Pi, and P. Sultan, "Onset conditions for equatorial spread F," *J. Geophys. Res.*, vol. 97, p. 13 865, 1992.
- [5] J. Aarons, "The longitudinal morphology of equatorial F-layer irregularities relevant to their occurrence," *Radio Sci.*, vol. 30, p. 631, 1993.
- [6] E. I. Thorsos, "The validity of the Kirchhoff approximation for rough surface scattering using a Gaussian roughness spectrum," *J. Acoust. Soc. Amer.*, vol. 83, no. 1, pp. 78–92, 1988.
- [7] S. Quegan and J. Lamont, "Ionospheric and tropospheric effects on synthetic aperture radar performance," *Int. J. Remote Sensing*, vol. 1, pp. 525–539, 1986.
- [8] K. C. Yeh, C. H. Liu, and S. J. Franke, "Manifestations of multiple scattering characteristics in transionospheric radio signals," in *Multiple Scattering of Waves in Random Media and Random Rough Surfaces*, V. V. Varadan and V. K. Varadan, Eds. University Park, PA: Pennsylvania State Univ. Press, 1986, pp. 291–310.
- [9] S. E. El-Khamy and R. E. McIntosh, "Optimum transionospheric pulse transmission," *IEEE Trans. Antennas Propagat.*, vol. AP-21, pp. 269–273, Mar. 1973.
- [10] A. Ishimaru, *Wave Propagation and Scattering in Random Media*. Piscataway, NJ: IEEE Press, 1997.
- [11] J. Liu, Y. Kuga, A. Ishimaru, and T. Freeman, "Simulations of ionospheric effects on SAR at P-band," in *Proc. IGARSS, Hamburg, Germany*, July 1999.



Jun Liu received the B.S. degree in atmospheric physics and the M.S. degree in atmospheric environment from the University of Science and Technology of China, Hefei, China, in 1991 and 1994, respectively. He received the MSEE degree in electrical engineering in 1999 and is currently pursuing the Ph.D. degree, both from the University of Washington, Seattle.

He is currently a Radio Frequency Engineer at Western Wireless Corp in Bellevue, WA. From 1999 to 2002, he worked as a Network Engineer at Metawave Communications, Redmond, WA. His research interests include electromagnetic scattering, wireless communications, radio frequency systems, and SAR systems.



Yasuo Kuga (S'92–M'83–SM'90) received the B.S., M.S., and Ph.D. degrees from the University of Washington, Seattle in 1977, 1979, and 1983, respectively.

He is currently a Professor of electrical engineering at the University of Washington. He has been with the University of Washington since 1991. From 1983 to 1988, he was a Research Assistant Professor of electrical engineering at the University of Washington. From 1988 to 1991, he was an Assistant Professor of electrical engineering and computer science at The University of Michigan, Ann Arbor. His research interests are in the areas of microwave and millimeter-wave remote sensing, high-frequency devices and materials, and optics.

Dr. Kuga has been an Associate Editor of *Radio Science* from 1993 to 1996 and an Associate Editor of the IEEE TRANSACTIONS ON GEOSCIENCE AND REMOTE SENSING from 1996 to 2000.



Akira Ishimaru (M'58–SM'63–F'73–LF'94) received the B.S. degree from the University of Tokyo, Tokyo, Japan, in 1951, and the Ph.D. degree in electrical engineering from the University of Washington, Seattle, in 1958.

From 1951 to 1952, he was with the Electrotechnical Laboratory, Tanashi, Tokyo, Japan, and in 1956, he was with Bell Laboratories, Holmdel, NJ. In 1958, he joined the faculty of the Department of Electrical Engineering, University of Washington, where he was Professor of electrical engineering and

Adjunct Professor of applied mathematics. He is currently Professor Emeritus there. He has also been a Visiting Associate Professor at the University of California, Berkeley. His current research includes waves in random media, remote sensing, object detection and imaging in clutter environment, inverse problems, millimeter wave and optical propagation and scattering in the atmosphere and the terrain, rough surface scattering, and optical diffusion in tissues. He is the author of *Wave Propagation and Scattering in Random Media* (New York: Academic, 1978; IEEE Press–Oxford University Press Classic reissue, 1997) and *Electromagnetic Wave Propagation, Radiation, and Scattering* (Upper Saddle River, NJ: Prentice-Hall, 1991).

Dr. Ishimaru has served as a member-at-large of the U.S. National Committee (USNC) and was Chairman (from 1985 to 1987) of Commission B of the USNC/International Union of *Radio Science*. He was Editor of *Radio Science* from 1979 to 1983 and was Founding Editor of *Waves in Random Media*. He is a Fellow of the Optical Society of America, the Acoustical Society of America, and the Institute of Physics. He was the recipient of the 1968 IEEE Region VI Achievement Award and the IEEE Centennial Medal in 1984. He was appointed as Boeing Martin Professor in the College of Engineering in 1993. In 1995, he was awarded the Distinguished Achievement Award from the IEEE Antennas and Propagation Society. He was elected to the National Academy of Engineering in 1996. In 1998, he was awarded the Distinguished Achievement Award from the IEEE Geoscience and Remote Sensing Society. He was awarded the 1999 IEEE Heinrich Hertz Medal and the 1999 URSI Dellinger Gold Medal. In 2000, he received the IEEE Third Millennium Medal.



Xiaoqing Pi received the B.S. degree in radio wave propagation and antennas in 1982 and the M.S. degree in space physics in 1985, both from Wuhan University, Wuhan, China. He received the Ph.D. degree in astronomy from Boston University, Boston, MA, in 1995.

He was a Research Associate at Boston University, Boston, MA, in 1995, and joined the Jet Propulsion Laboratory (JPL), Pasadena, CA, in 1996. He is currently a Senior Staff Member at JPL (since 2000) and a Research Associate Professor at the University of Southern California, Los Angeles (since 1998). He is a developer of the global assimilative ionospheric model and has led the development of JPL's ionospheric scintillation monitoring system network. He has been responsible for the ionospheric calibration for the U.S. Navy's GeoSat-Follow-On mission. His current research includes assimilative ionospheric modeling, ionospheric scintillation, ionospheric remote sensing, and mapping using the global positioning system, ionospheric effects on and modeling for satellite-based navigation systems including the U.S. wide-area augmentation system.

Dr. Pi was awarded the JPL NOVA award in 1997 and the NASA Certificate of Recognition Technical Awards in 1999 and 2000 for the development of global ionospheric monitoring and forecasting system. He is a member of the Institute of Navigation and the American Geophysical Union, and he serves as a member of Commission-G of the International Union of Radio Science.

Anthony Freeman (M'83–SM'94–F'00), photograph and biography not available at the time of publication.